Journal of
Marine Science and Engineering

MDPI

Article

Load Redistribution and Support Margins During Ship Launching with Gas Loss from a Single Airbag

Ji Chen [1,2], Saiful Bahri Mohamed [1,*] and Rongtao Yang [3]

[1] Faculty of Innovative Design and Technology, Universiti Sultan Zainal Abidin, Kuala Terengganu 21300, Terengganu, Malaysia
[2] School of Mechanical Engineering and Automation, Bohai Shipbuilding Vocational College, Huludao 125105, China
[3] Anhui Port & Shipping Sealand Equipment Co., Ltd., Hefei 230000, China
* Correspondence: saifulbahri@unisza.edu.my or wetk7121@outlook.com

Abstract

Airbag launching is widely used to put large hulls into the water, but its safety is normally assessed assuming an intact support array. This paper examines how gas loss from a single airbag redistributes vertical support and alters the remaining margin during a longitudinal bulk-carrier launch. The hull is modelled as a Euler–Bernoulli beam on compression-only airbags, each combining an isothermal gas term with a pressure-independent carcass stiffness calibrated against published model-scale tests, while buoyancy is integrated over the immersed stern until float-off. Three quantitative results define the contribution. First, the unfavourable support position is not at midship: it follows the slipway end, staying 0.8–5.1 m ahead of it, and the offsets are identical for 57,000, 100,000 and 180,000 deadweight-tonne hulls on the same bag array, so the critical location is a property of the launch arrangement rather than of the ship. Second, because the carcass stiffness is independent of the gas mass, gas loss is not a proportional capacity loss: a fully depressurised bag still carries 32% of its intact reaction (2.5 against 7.7 MN), and the usual proportional reduction at 40% gas loss understates the residual support by 16%. Third, the global safety factor falls from 1.357 to 0.796 and drops below 1.2 at a stern draught of 3.0 m, yet the governing limit is the working height rather than the bearing capacity, and it is exhausted only when eight adjacent bags are emptied, the margin turning to −0.014 m against a 0.60 m floor. The residual figures quoted above follow from the assumed carcass law and are not offered as design allowances.

Keywords: airbag launching; gas loss; load redistribution; support margin; quasi-static model; Euler–Bernoulli beam; minimum working height; multi-bag damage

Check for updates

Academic Editor: Md Jahir Rizvi

Received: 28 October 2026
Revised: 9 November 2026
Accepted: 11 November 2026
Published: 27 November 2026

Copyright: © 2026 by the authors. Licensee MDPI, Basel, Switzerland. This article is an open access article distributed under the terms and conditions of the Creative Commons Attribution (CC BY) license.

1. Introduction

Longitudinal launching on inflatable bags is now a routine method for putting hulls up to about 100,000 deadweight tonnes into the water, particularly where a dry dock is unavailable or uneconomic. The hull rests on a row of fabric-reinforced bags laid on an inclined slipway; as the ship is released it slides stern-first, the bags roll beneath the bottom and are recovered behind the stern, and the aft part of the hull enters the water while the forward part is still supported on the ways. The support system, rather than the hull structure, is usually the element that limits the operation, and its condition is assessed before the launch by calculation rather than by measurement.

The mechanics of the bag itself has received considerable attention, and the results matter for what a deflated bag can still carry. The composite construction of the bag, rubber

layers over cord plies, has been characterised by tensile testing and orthotropic constitutive models [1]. Inflated and cord-reinforced fabric tubes have been treated analytically [2] and tested on braided fabric beams and tubular members [3,4], and the wrinkling that precedes the failure of such a tube in bending has been analysed [5]. The bending and compression behaviour of drop-stitch fabric panels has been measured and modelled [6], and the additional contribution of shear deformation to their transverse response has since been quantified [7]; for marine membranes, the bending and failure behaviour of the inflated composite has been characterised specifically [8]. Two conclusions from this group bear directly on the present problem. The compressive reaction of an inflated bag is generated mainly by the pressure acting on the contact area, and the reinforcement contributes a smaller share that changes little with pressure, so a bag that has lost gas is not a bag with proportionally reduced capacity. Additionally, the fabric share becomes relatively more important as the bag flattens, which is the state in which a damaged bag is asked to work.

The contact between a bag and the hull bottom has been solved for an array of bags as a nonlinear coupled problem [9], and the rigidity of a compressed bag has been measured and built into safety assessments [10]. At the level of the arrangement, the laying of bag arrangements for barge launching has been investigated numerically [11], a passenger ship launch has been designed using an airbag system [12], and a 330 ft barge launch has been calculated and carried out in accordance with the Chinese shipbuilding standard CB/T 3837-1998 [13]. The structural consequence of the arrangement has also been examined in a finite element analysis of a wooden Pinisi hull, in which the launching system appears as a set of discrete supports [14]. Technical and economic comparisons between slipway and airbag launching complete this group [15,16]. What these studies have in common is their question: whether a given arrangement, treated as intact, provides enough capacity, and how the hull responds to the support pressures that the arrangement produces.

At the level of the whole ship, launching has been analysed through automated quasi-static equilibrium procedures [17] and longitudinal stability formulations [18], through dynamic and URANS simulations of the launch [19], through data-driven control of jacket launches [20], and through calculation procedures that follow the launch from the first movement to float-off [21]. The most recent of these raise the fidelity of the hydrodynamic and dynamic description rather than that of the support: ref. [19] resolves the transient motion of a large container ship in the water, and [20] replaces the launch calculation by a learned model for a jacket, but in both cases the bags are intact and their internal pressure is fixed. The structural side shows the same division: hull-girder ultimate strength continues to be refined through Smith-type progressive collapse with elastic shakedown [22], whereas the support state against which that strength is compared is taken as uniform. Risk-based treatment of the operation [23], general accounts of launching practice [24], the rolling resistance of the bags on the slipway [25], the keel-block arrangements used for hulls with large overhangs [26], and the standard that fixes the design values [27] complete the picture of how a launch is assessed at present.

Reduced internal pressure has so far been treated as a property of the bag rather than of the support system. The nonlinear rigidity of the compressed bag was introduced into a launch safety assessment by Ren et al. [10], and the contact coupling of a complete array was solved by Liu and Yu [9], so the internal pressure is already a variable of the intact calculation. The failure of a bag has been analysed at the level of the bag itself. Liu et al. [28] coupled smoothed particle hydrodynamics with the finite element method and a Hashin criterion to follow membrane fracture and the escaping jet and found that a burst initiates where the bilge bears on the bag and that a potential burst in some bags raises the stress of the hull section appreciably. Li et al. [29] represented an extreme burst within a dynamic model of the launch and assessed its consequence for the process, and risk analyses of the

operation list pressure loss among the failure modes to be managed [23]. These studies establish that a burst is credible and locally severe, but they treat the damaged bag as one that has failed rather than as a support element whose remaining capacity still depends on its compression. The two quantities that a launch assessment needs are therefore not available: the capacity actually lost by the damaged bag, and the margin that remains in the array. Neither follows from the gas ratio, because the pneumatic and carcass contributions to the reaction are additive but not proportional (Section 2.3); the gas supplies about 70 per cent of the reaction at the working height, so its loss removes capacity in a way that the gas ratio alone cannot express. It is these two quantities that this paper computes.

In practice the event is foreseeable rather than exceptional, but its frequency cannot be quantified from published data: no consolidated incident record for airbag launching is available, and the evidence available is qualitative. The design values that govern the operation, by contrast, are specified for the intact array [27]. What makes the event consequential is the absence of redundancy. Each bag carries only a few per cent of the launching weight, but the bags are discrete parallel supports with no back-up, so the share released by one bag is transferred to its neighbours, and the array holds no reserve other than the margin built into its safety factor. Current assessments, however, test that margin only for the normal configuration: the allowable internal pressure, the rated load per unit length and the global safety factor are checked for an intact array, and no check asks what the array can still carry after a bag has lost gas, how the released share is redistributed along the hull, or how much working height remains before the bottom reaches the ways. Those are the three quantities computed in this paper.

Two features remain common to this body of work. First, apart from the burst studies just cited, the array is treated as intact: either every bag is assumed to carry its share, or the analysis is a normal-operation one in which the possibility of a bag losing pressure is not represented. Second, where a damaged bag is considered at all, it is represented by reducing its bearing capacity in proportion to the loss of gas, which is convenient but not justified by the mechanics of a cord-reinforced bag. Neither assumption has been tested against a model in which gas mass and fabric load path are represented separately. Stated in one sentence, the literature explains how an intact array carries a hull and how a single bag fails, but not what a hull on a partly deflated array can still carry; that is the gap addressed here.

This paper addresses the following two questions. First, how does the loss of gas from a single bag redistribute the vertical support along the hull, and which support position governs the remaining margin as the launch proceeds? Second, is the common proportional reduction of capacity admissible, or does it misstate the residual support of a damaged bag? The answers matter for the field as well as for this case. The values against which a launch is checked, namely the allowable pressure, the rated load per unit length and the global safety factor, are all specified for an intact array [27], and the analyses reviewed above likewise evaluate intact configurations; a residual support that can be computed from the same quantities therefore allows a damaged array to be assessed without a new acceptance criterion, and it indicates where along the hull that assessment should be applied.

To answer them, a quasi-static model is formulated in which the hull is represented by an elastic Euler–Bernoulli beam, each bag by a compression-only support consisting of an isothermal gas term and a cord-reinforced carcass term, and the immersed stern by a buoyancy distribution. The slipway end is advanced along the hull so that bags leave the ways in sequence, which allows the support configuration to be followed through the launch rather than evaluated at a single instant. The carcass stiffness is calibrated on published model-scale bearing tests and cross-checked against the manufacturer's rating; the numerical

implementation is verified against closed-form beam solutions, a mesh-refinement study and an independent equilibrium audit.

The contributions are threefold. First, the analysis shows that the unfavourable support position migrates with the launch stage and stays at the slipway boundary, so that neither midship nor any fixed station is the critical location; the same offsets are recovered for 57,000, 100,000 and 180,000 DWT hulls, which identifies the position as a property of the launch arrangement rather than of the ship. Second, it quantifies the separation between gas loss and capacity loss and expresses it in closed form, so that the error of a proportional reduction can be stated rather than assumed. Third, it identifies which indicator governs: local utilisation peaks early in the launch and then relaxes, whereas the system reserve falls throughout, and under multi-bag loss the first limit reached is the minimum working height rather than the bearing capacity. The scope is deliberately restricted to the quasi-static phase; inertia, slipway friction and the transient following a bag burst are not modelled, and the reasons are discussed in Section 5.4.

The contributions should be separated from the elements that this paper borrows. The elastic-beam idealisation, the compression-only support, the isothermal gas law and the cord-reinforced carcass law are all established; the launch analyses of Liu and Yu [9] and Ren et al. [10] already treat the complete array as a coupled system with a nonlinear bag law, and the burst simulation of Liu et al. [28] resolves a single bag down to membrane failure. What these formulations do not supply is a relation between the gas remaining in a bag and the support that the same bag continues to give the hull, maintained through the launch: the intact analyses evaluate successive instants of an undamaged array, and the bag-level study returns no residual capacity to the support sequence. The present model is built to supply that relation, and the difference is one of what can be answered rather than only how accurately. Once gas mass and carcass load path are represented in the same element, the residual support of a damaged bag becomes a computed rather than an assumed quantity, the error of a proportional reduction becomes expressible in closed form (Section 5.1), and the limit reached first under multi-bag loss can be identified rather than postulated. To the authors' knowledge, no published launch analysis reports the governing support position as an offset from the slipway end or shows that this offset is unchanged across hull sizes; that result follows from advancing the support configuration through the launch instead of evaluating a single instant, and it is the basis on which the reserve can be monitored at a predicted location rather than at a fixed station.

2. Model

2.1. Problem Statement and Assumptions

The launch is treated as a sequence of quasi-static equilibrium states of the hull resting on an array of airbags that lie on an inclined slipway, with the aft part of the hull progressively entering the water. Figure 1 shows the arrangement and the idealisation adopted. The following assumptions are made:

1. Vertical equilibrium only; inertia, longitudinal motion, and slipway friction are neglected, so the analysis applies to the slow quasi-static phase before any dynamic run-out.
2. Gas loss is described by the residual mass ratio $\mu = m/m_0$ of a single bag, where m is the mass of gas remaining and m_0 its initial value; the leakage rate and the accident chronology are outside the scope of the model.
3. The bag behaves as a closed volume of gas at constant temperature whose pneumatic load scales with the isothermal compression of the enclosed volume, while the multi-ply cord-reinforced rubber carcass contributes a structural contact stiffness independent of the internal gas mass.

4. The bag cross-section flattens at constant perimeter, which fixes the contact width and the enclosed volume as functions of the working height.
5. Buoyancy is integrated over the immersed length using an equivalent waterline breadth; the free surface is horizontal in the world frame.

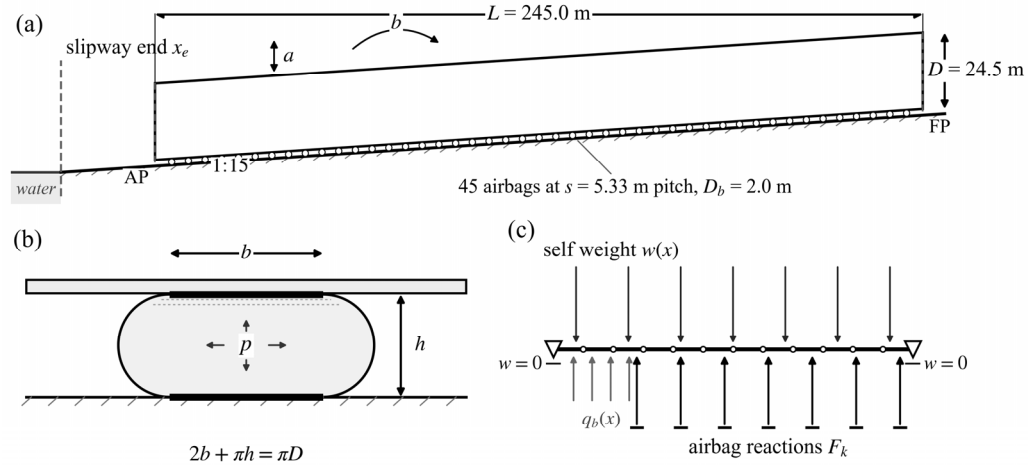

Figure 1. Schematic of the model: (**a**) general arrangement of the representative vessel on the airbag array, drawn to scale (length 245.0 m, depth 24.5 m; 45 bags at 5.33 m pitch and 2.0 m diameter), in which a is the rigid-body heave and b the pitch; (**b**) compressed section of a single airbag; (**c**) mechanical model used in the analysis.

Each assumption enters the results at a specific point. The quasi-static treatment replaces the launch history by a sequence of equilibrium states, so the reactions and margins reported are those of each configuration and carry no dynamic amplification: the stage sequence, not the time axis, is what organises the results of Section 4. The residual mass ratio makes the outcome a function of the state of the bag rather than of the time needed to reach it, which is why a loss of a given fraction produces the same redistribution whatever the leakage rate. The isothermal gas term and the gas-independent carcass term together produce the non-proportional residual of Sections 4.3 and 4.4; if the carcass term also scaled with the enclosed gas mass, the residual would be proportional and the central result would disappear. The constant-perimeter flattening fixes both the contact width and the enclosed volume as functions of the working height, so the reaction depends on height alone, and because the intact and damaged states share the same geometric law an error in that law largely cancels when the residual is taken as a ratio. The equivalent waterline breadth changes how the launching weight is divided between water and bags, and hence the absolute level of reaction, but not the longitudinal transfer of load that the paper reports.

These idealisations are consistent with the conditions of a real launch. The operation is slow, and the hull passes through a continuous succession of equilibrium states, which is the idealisation adopted by the calculation procedures of [17,21]; the dynamic phase is confined to the run-out after the hull has left the ways, which lies outside a study of support margins. The bag exchanges heat with the water and the surrounding air over the whole launch and its internal pressure varies only between 0.15 and 0.35 MPa, so the isothermal reading is appropriate, while the carcass stiffness is carried by the cord plies and is therefore indifferent to gas mass, as the manufacturer rating and the calibration of Section 3.2 both indicate. Flattening at constant perimeter is the standard kinematic assumption for an inextensible fabric envelope, and it is the basis on which bag capacity is rated at a given working height. Calm water is the condition under which these launches are performed. The treatment of gas loss as a state rather than a rate is the departure that matters most, since a real tear deflates a bag quickly; it is retained because the endpoint

governs the residual support, and the fully emptied bag is included among the cases of Section 4.5, so a faster path ends in a state that has already been analysed. What the model does not reproduce is the transient load spike during deflation, which is a dynamic effect and is identified as such in Section 5.4.

2.2. Hull Beam and Equilibrium

The hull is discretised into two-node Euler–Bernoulli elements with vertical displacement w and rotation θ at each node. The bending stiffness $EI(x)$ represents the hull-girder flexural rigidity along the length (taken as a uniform effective value in the present parametric study). The total vertical displacement of the keel line is split into a rigid body part and an elastic part,

$$Y(x) = a + b\,(x - x_{mid}) + w(x) \tag{1}$$

where a is the heave, b the pitch and $w(x)$ the elastic deflection obtained from the beam elements. The rigid-body part is referred to midship: x_{mid} is the longitudinal coordinate of midship and $Y(x)$ the total vertical displacement of the keel line. The array of bags acts as a set of discrete elastic supports, for which the equivalence to a beam on an elastic foundation is established in [30], and for which unsteady formulations are also available [31]. The rigid-body modes of the beam are removed by two gauge pins ($w = 0$ at the fore and aft ends), so that the elastic problem is non-singular, while the two rigid-body amplitudes are determined by global equilibrium:

$$\sum F = 0, \qquad \sum M = 0 \tag{2}$$

Only physical loads enter Equation (2), namely self weight, airbag reactions and buoyancy, so the gauge-pin reactions vanish identically once Equation (2) is satisfied and the pins do not alter the solution.

The choice of this beam idealisation follows from the proportions of the problem and from the precedent set by earlier launching analyses. A bulk-carrier hull is a slender thin-walled box girder whose depth-to-length ratio is about 1:10 (Table 1); for such a girder the shear contribution to the global deflection scales with the square of that ratio and is small compared with the bending term, so Euler–Bernoulli kinematics retain the dominant deformation while discarding a correction that does not affect the support forces reported here. The same reduction underlies the beam-on-elastic-foundation treatment of bag-supported hulls [30] and the unsteady beam formulations used for the same class of problem [31]. The loading is also smooth at the scale of the hull: bag reactions act at a pitch of 5.33 m, so that about 45 supports share the launching weight over 245 m, and the bending moment therefore varies over a length several times that pitch. Transverse and local effects, such as plate bending between bags, shell buckling beneath a single bag and the stress concentration at the slipway end, are not resolved by this idealisation and lie outside the support-margin question addressed here (Section 5.4).

The external loads are assembled as consistent nodal forces. The self weight is prescribed as a longitudinal distribution whose first moment matches the specified centre of gravity; buoyancy is applied as

$$q_b(x) = \rho g\, B(x) \max\,(0,\, z_w - z_k(x) - Y(x)) \tag{3}$$

with ρ the density of water, g the gravitational acceleration, z_w the waterline elevation, z_k the keel elevation and $B(x)$ the equivalent waterline breadth.

Table 1. Principal particulars of the representative vessel and specification of the airbag system.

Item	Symbol	Value	Unit
Length between perpendiculars L	L	245	m
Breadth moulded	B	43	m
Depth moulded	D	24.5	m
Block coefficient	C_b	0.85	-
Lightship weight	W_L	21,500	t
Launching weight	W	23,200	t
Longitudinal centre of gravity from AP	x_g	115.0	m
Slipway slope	α	1:15	-
Airbag free diameter	D_b	2.0	m
Airbag effective length	L_b	18.0	m
Number of airbags	N	45	-
Longitudinal airbag pitch	s	5.33	m
Initial inflation pressure (at V_0)	p_0	0.15	MPa
Allowable pressure	p_{allow}	0.35	MPa
Rated capacity per unit length	q_{rated}	450	kN/m
Design safety factor on capacity	SF0	1.5	-
Maximum allowable deformation	δ_{max}	1.4	m
Minimum working height	h_{min}	0.60	m
Ultimate capacity per airbag	F_{ult}	12.15	MN
Carcass stiffness	k_s	136	kPa

2.3. Airbag Support Model

A bag of free diameter D_b and effective length L_b compressed to a working height h is idealised as a rectangle of width b closed by two semicircles (Figure 1b). Constant perimeter gives

$$b(h) = \frac{\pi}{2}(D_b - h), \qquad A_{cs}(h) = bh + \frac{\pi h^2}{4} \tag{4}$$

where A_{cs} is the cross-sectional area. The enclosed gas volume and the contact area with the hull bottom are the products $V(h) = A_{cs}L_b$ and $A(h) = bL_b$. The reaction is written as the sum of a gas term and a carcass term,

$$F(h) = \mu\, p_0 \frac{V_0}{V(h)} A(h) + k_s\,(D_b - h)\,L_b \tag{5}$$

and is truncated at the ultimate capacity F_{ult} so that a fully flattened bag cannot mobilise an unbounded reaction. A bag that has slipped off the ways carries no load, and a bag whose height exceeds D_b is out of contact. In Equation (5), p_0 and V_0 are the initial internal pressure and enclosed gas volume of the bag, and μ is the residual mass ratio defined in Section 2.1.

The carcass stiffness k_s characterises the structural resistance of the multi-ply cord-reinforced rubber wall under contact flattening and is calibrated in Section 3.2 against published model-scale tests. The point of Equation (5) is that k_s does not depend on μ: gas loss reduces the pneumatic term only, so the bearing capacity of a depressurised bag is not proportional to its gas content.

2.4. Launch-Stage Parameterisation

Two parameters describe a launch stage. The position of the slipway end in hull coordinates, x_e, defines the effective support boundary behind which ($x < x_e$) the bags have already left the load-bearing ways and therefore provide no support. The waterline elevation z_w defines the immersed length. Referencing the way-end termination to the waterline datum links the two kinematically by $d = x_e \tan\alpha$, where d is the stern draft and α

the slipway slope, so that advancing the hull past the slipway end and immersing the stern are driven by a single stage parameter.

A unilateral Winkler contact is also defined between the hull bottom and the ways so that the solution remains bounded if a bag is compressed to zero height. In the stages reported here, up to $d = 5.0$ m, this contact is never activated, which is itself an outcome of the analysis. Beyond that draft the floatation balance is reached and the bags unload completely, so the stage no longer belongs to the bag-supported phase modelled here.

2.5. Simplified Capacity-Reduction Model

Engineering assessments frequently replace a damaged bag by one with a reduced capacity. In Simplified A the reaction of the intact bag is scaled by a factor λ_A chosen so that the capacity matches the gas-loss model at a reference working height h_{ref}, which gives

$$\lambda_A = \frac{\mu\, p_0 V_0 A\left(h_{ref}\right)/V\left(h_{ref}\right) + k_s\left(D_b - h_{ref}\right)L_b}{p_0 V_0 A\left(h_{ref}\right)/V\left(h_{ref}\right) + k_s\left(D_b - h_{ref}\right)L_b} \tag{6}$$

In Simplified B the gas-loss ratio is taken directly as the capacity ratio, $\lambda_B = \mu$, which is the assumption implicitly made when gas loss is equated with loss of bearing capacity.

Because Equation (5) is a sum of a μ-proportional term and a μ-independent term, $\lambda_A > \mu$ whenever $k_s > 0$, and the two variants bracket the plausible range of engineering practice. Figure 2 shows the resulting relations for the full-scale bag: panel (a) gives the reaction-height curves of the four states considered, and panel (b) plots the capacity ratio against the residual gas mass ratio, the region underestimated by the proportional reduction being shaded. The gap opened up by the proportional reduction is the carcass share of the reaction, and it widens monotonically as the loss increases.

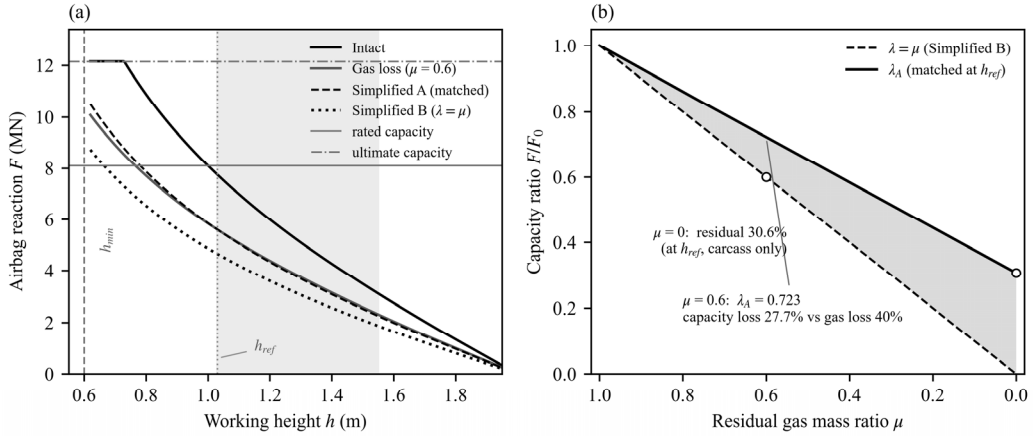

Figure 2. (**a**) Reaction-height relation of the full-scale bag for four support states: intact; uniform gas loss leaving 60% of the initial gas mass; Simplified A, the intact curve scaled by a factor matched at the reference height of 1.031 m; Simplified B, the intact curve scaled by the residual gas ratio itself. The grey band spans the working heights of the loaded bags at the governing stage. (**b**) Capacity ratio against residual gas mass ratio at the reference height, with the region understated by the proportional reduction shaded.

Panel (a) repays a closer reading, because the four states differ in construction as well as in level. The intact curve is the reference. Uniform gas loss that leaves 60% of the initial gas mass scales the pneumatic term alone and leaves the carcass term intact, so at the reference height of 1.031 m the reaction falls from 7.74 MN to 5.59 MN, a capacity loss of 27.7% for a gas loss of 40%. The missing 12.3 percentage points are the carcass share of the intact reaction, 30.6%, multiplied by the gas actually lost, and the decomposition holds at every height: the carcass share falls to 22.7% at the minimum working height of

0.6 m and the relative error of a proportional reduction narrows from 12 to 9 percentage points. Simplified A scales the whole intact curve by one factor, 0.723, chosen to reproduce the gas-loss reaction at the reference height. The two curves coincide there, but a uniform scaling cannot reproduce how the pneumatic and carcass terms vary with height separately, so A is about 5% steeper than the gas-loss curve at the reference height and 0.4% high at the 49 mm settlement the bag reaches when it is empty. Simplified B scales by 0.6 itself, which places it 0.95 MN, or 17%, below the gas-loss curve at the reference height and makes it the softest of the four states. The grey band in the panel spans the working heights of the 37 loaded bags at the governing stage, 1.03–1.55 m, so it marks the interval over which these differences are actually exercised.

Panel (b) reduces the same information to the quantity a simplified assessment uses, the capacity ratio at the reference height. Because the carcass term is indifferent to gas mass, the capacity ratio lies above the residual gas ratio by the carcass share multiplied by the gas lost: 0.723 against 0.60 at the present loss, and a residual of 30.6% when the bag is completely deflated, which is the intercept of the matched curve in the panel. The shaded region is therefore not a plotting artefact but the support that a proportional reduction cannot see. Two points about its use should be stated. One, the ratio is evaluated at a fixed reference height, whereas in the launch the damaged bag settles, by 19 mm at 40% gas loss and by 49 mm when empty, and this settlement lifts the residual to 32% of the intact reaction, so the panel is marginally conservative in that respect. Two, the matched factor depends on the height at which the match is made: over the working band of the array, it varies only between 0.723 and 0.742, so the choice of reference height moves the third significant figure but neither the sign nor the order of magnitude of the error. What the two panels establish for the rest of the paper is that proportionality is an assumption about the bag rather than a consequence of gas loss, and that its error is zero at no loss and bounded above by the carcass share of the reaction. Both the settlement and the resulting figure are consequences of the linear carcass law over the deformation range of Section 3.2, and neither is a design allowance.

2.6. Numerical Solution

The unknowns are the nodal deflections and rotations w and θ, together with the two rigid-body parameters a and b of Equation (1). The residual vector combines the beam equilibrium equations with Equation (2) and is solved by Newton–Raphson iteration with an analytic tangent matrix and a backtracking line search. With the unknowns collected in the vector u, the residual, the update and the convergence test are written as

$$R(u) = Ku - f(u) = 0 \tag{7}$$

$$J(u^k)\Delta u^k = -R(u^k),\ u^{k+1} = u^k + \Delta u^k \tag{8}$$

$$\frac{\|R(u^k)\|}{W} \leq 10^{-8} \tag{9}$$

in which u is the vector of unknowns, K the elastic stiffness matrix assembled from the elements of Section 2.7 and f the consistent nodal load vector from self weight, bag reactions and buoyancy; J is the tangent matrix, the derivative of the residual vector R with respect to u. Bags that enter or leave contact change the tangent discontinuously, so the stage sequence is solved by continuation, each stage starting from the previous solution. The waterline of each stage is itself a fixed-point problem, $d = z_w - Y(0)$, and is iterated until the correction falls below 10^{-4} m; with that criterion every reported stage converges in two to thirty-six iterations. The equilibrium residual is accepted below 10^{-8} of the launching weight, the tolerance of Equation (9). Verification against closed-form beam solutions, a mesh-refinement study and an independent global equilibrium audit is reported in Section 3.3.

2.7. Discretisation and Stage Sequence

The hull is discretised into two-node Hermite Euler–Bernoulli elements with two degrees of freedom per node, the vertical deflection and the rotation, and a constant flexural rigidity within each element, equal to the effective value fixed in Section 3.1. The mesh is uniform at 1 m, giving 245 elements over the 245 m length between perpendiculars; the refinement study behind that choice is reported in Section 3.3. The weight and the buoyancy are converted to consistent nodal loads with three-point Gauss integration. A bag rarely coincides with a node at a pitch of 5.33 m, so it is located inside its element and its reaction is distributed to the two nodes by linear interpolation of the nodal deflections; the support force and the structural stiffness therefore act on the same displacement field.

Because the launch is treated as quasi-static, no time step exists in this calculation: each stage is a separate equilibrium state and the solution is a continuation in the stern draft rather than an integration in time. Stages are 0.5 m of stern draft apart, which advances the slipway end by 7.5 m, about 1.4 bag pitches, so that at most two bags pass the end between consecutive stages. Since every stage is converged to equilibrium rather than incremented, the step length governs only how densely the envelopes of Figure 3 and Figure 4 are sampled, not the accuracy of the states that are reported. A time step would enter only in the dynamic phase after float-off and in the transient following a burst, both of which lie outside the scope stated in Section 5.4.

2.8. Isothermal Idealisation and Gas-Loss Rate

The gas term follows $p(h) = \mu\, p0\, V0/V(h)$, the isothermal form of the gas law, with $\mu = m/m0$ the fraction of the initial mass retained. Because both $V(h)$ and $A(h)$ are taken from the equal-perimeter section of Section 2.3, the interaction of a gas loss with the bag geometry is inside the support law rather than beside it: as the bag flattens, its volume falls faster than its contact area grows, the pressure rises, and the reaction falls by less than the mass. The gas term and the carcass term therefore respond to the loss in different proportions, which is why the residual is not proportional (Section 5.1).

The pressure is read at constant temperature. The physical grounds are set out in Section 2.1; the quantitative consequence, which is what matters for the margins, is that the isothermal choice is the softer of the two limits. At the most compressed state of the present case, $h = 0.60$ m and $V/V0 = 0.51$, an adiabatic exponent of 1.4 would give a gas pressure 31% higher and a correspondingly larger reaction, so the predicted working heights and margins are not optimistic. No measured wall temperature of a bag in a launch was found in the sources reviewed, and that absence is listed in Section 5.4.

The discharge itself is not resolved and no discharge rate is prescribed. The residual mass is set at the stage of interest and the equilibrium is then solved, because what the hull feels at that instant depends on how much gas remains rather than on how quickly it left; the deflation transient is a dynamic effect and lies outside the quasi-static scope stated in Section 5.4. A discharge history would require an orifice area and a leak law that are not available for launching conditions, whereas the three values examined run from a partial loss to complete emptying.

3. Case Study and Verification

3.1. Representative Vessel and Airbag Array

The example is a 100,000 DWT class bulk carrier, with the principal particulars listed in Table 1. The vessel is a representative hull of this class rather than a specific existing ship, and its particulars in Table 1 define the parent-design basis of this study: the principal dimensions ($L/B = 5.70$, $B/D = 1.76$, block coefficient $Cb = 0.85$ and a lightship-to-deadweight ratio of 0.21) are representative of 100,000 DWT bulk carriers. No shipyard drawing, owner's

loading data or measured value is used, so every hull input required to repeat the calculation is listed in Table 1. The launching weight W is 23,200 t, the lightship weight W_L is 21,500 t and the longitudinal centre of gravity x_g is located 7.5 m aft of midship, which is typical of this ship type in the launching condition. Forty-five airbags ($N = 45$) of 2.0 m free diameter D_b and 18 m effective length L_b are spaced at a pitch s of 5.33 m along the length, so the array covers the hull from 5.33 m to 239.85 m measured from the aft perpendicular. The slipway slope is 1:15, within the 1:12 to 1:24 range used in practice. The bag rating used in the analysis is $q_{rated} = 450$ kN/m at the rated working height, with $p_0 = 0.15$ MPa, an allowable pressure p_{allow} of 0.35 MPa, a maximum allowable deformation δ_{max} of 1.4 m, a minimum working height h_{min} of 0.60 m and a design safety factor SF0 of 1.5 on the rated capacity (Table 1). Figure 1a shows this arrangement drawn to scale, including the 245.0 m hull length, the 24.5 m depth, the 5.33 m bag pitch and the 2.0 m bag diameter.

The longitudinal weight distribution is prescribed as a continuous hull-weight profile whose first moment reproduces the stated centre of gravity, with a concentration over the cargo-hold region and a secondary peak at the engine room. Its peak-to-mean ratio is varied as a parameter in Section 4.5, because it controls the location of the load maximum. The effective hull-girder bending stiffness is set to $EI = 4.0 \times 10^{13}$ N·m^2, which corresponds to a midship section modulus of about 16 m^3 at the moulded depth, within the range reported for hulls of this size [32]; the corresponding uncertainty in the hull girder strength is discussed in [33]. All input parameters are summarised in Table 1. The weight profile and the bending stiffness are therefore modelling inputs rather than measured ship data; their basis is stated here so that the case can be reconstructed and so that their influence can be assessed, as is done for the weight profile in Section 4.5.

3.2. Constitutive Calibration

The carcass stiffness k_s is the only parameter of Equation (5) that is not fixed by the manufacturer's data. It was calibrated against the model-scale bearing tests reported by Yu et al. [1], in which a 0.6 m diameter bag of 1.8 m length, inflated to 0.05 MPa, was compressed in an 800 t hydraulic press. At half compression the measured reaction is about 130 kN; forcing the model through this point gives $k_s = 1.36 \times 10^5$ Pa.

Two independent checks follow. First, the same k_s applied to the full-scale 2.0 m bag gives 450.2 kN/m at 50% deformation, against a rated capacity of 450 kN/m quoted by the manufacturer, a deviation of +0.04% (Table 2). The rated value played no part in the calibration, so the agreement is not circular. Second, at 70% deformation the model gives 837 kN/m, 24% above the rated capacity multiplied by the stated design safety factor SF0 of 1.5; this indicates that the manufacturer's ultimate value corresponds to roughly 63% deformation in the model, which is consistent with the specified maximum deformation of 1.4 m.

The 24% figure deserves a precise reading, because the reference it is measured against is not a test result. The third row of Table 2 compares the model with the rated working capacity multiplied by the stated design safety factor SF0 of 1.5, that is, with a linear extrapolation of capacity from 50% to 70% deformation. The present law does not extrapolate linearly: over the same interval the computed reaction grows by a factor of 1.86 rather than 1.5, because the pneumatic term varies as the inverse of the enclosed gas volume while the contact area grows as the bag flattens. The 24% is therefore the difference between two growth laws rather than a mis-fit at a data point, and at the calibration point itself the deviation is +0.04%. Nothing in the results of Section 4 depends on this row: the margins are formed as ratios between states evaluated with one and the same law, so a deviation of this kind cancels to first order, while the figure is still reported here because it delimits the validity of the constitutive model (Section 5.4).

Table 2. Constitutive calibration. The first row is the calibration basis; the remaining rows are independent anchors and were not used in fitting.

Case	Condition	Reference	Present Model	Deviation
Model-scale bag (Yu et al. [1]), 50% compression—calibration point	D_b = 0.6 m, L_b = 1.8 m, p_0 = 0.05 MPa	130 kN (digitised)	130.0 kN	calibration basis
Full-scale bag, 50% deformation—rated-capacity anchor	D_b = 2.0 m, L_b = 18 m, p_0 = 0.15 MPa	450 kN/m	450.2 kN/m	+0.04%
Full-scale bag, 70% deformation—ultimate-capacity anchor	D_b = 2.0 m, L_b = 18 m, p_0 = 0.15 MPa	675 kN/m (rated × SF0)	837.2 kN/m	+24.0%

The model was also evaluated across all four high-compression model-scale cases reported by Yu et al. [1], covering extreme compressions between 62% and 83%. Over that regime, deviations range from −42.2% to +7.3%, because progressive membrane lock-up stiffens the physical bag nonlinearly as it approaches complete flattening. The deformation in the present launching case ranges from 38% to 51% (Section 4.1), well within the moderate-compression regime anchored by the 50% calibration point, and the linear carcass relation understates the reaction through most of that range, exceeding the measured value only once the bag approaches complete flattening. The scope of this linearised representation is discussed further in Section 5.4.

3.3. Numerical Verification

Four checks were performed (Table 3). A cantilever with a tip load reproduces $PL^3/3EI$ to a relative error of 5×10^{-10}, and a simply supported beam under uniform load reproduces $5qL^4/384EI$ to 1×10^{-10}; both exercise the element formulation, the consistent nodal loads and the two-pin gauge arrangement used in the launch model. Refining the mesh from 122 to 490 elements changes the maximum airbag reaction by less than 10^{-5} relative (5.6015 MN in all three discretisations), so the 1 m mesh used throughout is adequate. The discretisation behind these numbers is the one set out in Section 2.7: two-node Hermite elements with two degrees of freedom per node, a constant flexural rigidity per element, equal to the effective value of Section 3.1, consistent nodal loads from three-point Gauss integration, and a bag reaction interpolated to the two nodes of the element that contains the bag. Finally, the global force and moment sums are recomputed from the output rather than from the solver internals, and both close below 10^{-12} of the launching weight. The Newton iteration converges in five to eleven steps with a residual below 10^{-9} of the launching weight.

The agreement in Table 3 is close to machine precision for the closed-form checks and below 1×10^{-5} for the mesh study, and this warrants an explanation rather than a claim of accuracy. In the two beam cases the element formulation reproduces the analytical solution exactly, because a uniform mesh with consistent nodal loads integrates the cubic and quartic fields without error; the residual deviations of order 1×10^{-10} are floating-point round-off, so these checks verify the assembly of the stiffness matrix, the gauge-pin constraint and the load vector rather than the accuracy of the interpolation. In the mesh study, which is run on the intact reference state, the reaction profile varies over tens of metres, whereas the bag pitch of 5.33 m is already resolved by five elements, so halving the element length changes the peak reaction by less than 5×10^{-6} in relative terms and the elastic deflection by 0.03 per cent; the 1 m mesh is therefore converged for the quantities reported here. Both groups are code verification against analytical or self-consistent references rather than experimental

validation: the constitutive law is calibrated on model-scale tests (Section 3.2), and the damaged-bag response remains experimentally unverified (Section 5.4).

Table 3. Verification of the numerical implementation.

Check	Result	Reference	Deviation
Cantilever, tip load: $PL^3/3EI$ (deflection)	3.333333×10^{-2} m	3.333333×10^{-2} m	5.0×10^{-10}
Cantilever, tip load: $PL^2/2EI$ (rotation)	5.000000×10^{-3} rad	5.000000×10^{-3} rad	4.9×10^{-10}
Simply supported, uniform load: $5qL^4/384EI$ (deflection)	1.302083×10^{-2} m	1.302083×10^{-2} m	1.1×10^{-10}
Mesh 122 elements: max bag reaction	5.601496 MN	5.601470 MN (245 elements)	4.6×10^{-6}
Mesh 245 elements: max bag reaction	5.601470 MN	reference	-
Mesh 490 elements: max bag reaction	5.601468 MN	5.601470 MN (245 elements)	3.4×10^{-7}
Mesh 122 elements: min working height	1.005690 m	1.005693 m (245 elements)	2.8×10^{-6}
Mesh 490 elements: min working height	1.005694 m	1.005693 m (245 elements)	2.1×10^{-7}
Mesh 122 elements: max utilisation	0.569275	0.569274 (245 elements)	1.8×10^{-6}
Mesh 490 elements: max utilisation	0.569274	0.569274 (245 elements)	1.4×10^{-7}
Mesh 122 elements: max elastic deflection	94.599 mm	94.576 mm (245 elements)	2.4×10^{-4}
Mesh 490 elements: max elastic deflection	94.570 mm	94.576 mm (245 elements)	6.1×10^{-5}
Global equilibrium audit ($\Sigma F/W$)	$<1 \times 10^{-12}$	0	-

4. Results

4.1. Stage Evolution of the Support System

Figure 3 and Table 4 summarise the launch as a function of stern draft d. As the hull advances, the bags leave the slipway one after another, and the number of bags still on the ways falls from 45 to 31 over the range examined (Table 4). No bag inside the slipway region loses contact, so the support area shrinks only because the array is progressively left behind, not because the hull lifts off the bags. The sequence is reported up to $d = 5.0$ m, where buoyancy already carries 42% of the launching weight; beyond that draft the floatation balance is reached and the bags unload completely, so the stage no longer belongs to the bag-supported phase this model addresses.

Three quantities are reported for every stage, and they are defined here rather than left to the table. With the allowable pressure of 0.35 MPa and the contact area defined in Section 2.3, the allowable reaction of a bag, the local utilisation of that bag and the safety factor of the array are

$$F_{allow,i} = p_{allow} A(h_i) \tag{10}$$

$$\mu_i = \frac{F_i}{F_{allow,i}} \tag{11}$$

$$SF(d) = \frac{\sum_{i \in \text{contact}} F_{allow,i}}{W} \tag{12}$$

Equation (12) is normalised by the launching weight of 227.5 MN, not by the load the bags happen to carry. The two are connected by vertical equilibrium: at each stage the reactions of the bags in contact and the buoyant force together balance the weight, so that

the sum of the reactions equals the weight less the buoyancy. Buoyancy therefore relieves the bags without restoring any reserve, while the numerator of Equation (12) falls as bags leave the ways. This is why the safety factor decreases monotonically from 1.357 to 0.796 through the sequence, whereas the local utilisation of Equation (11) rises and falls as the load is redistributed among the remaining support.

The three quantities listed in Table 4 evolve as follows. The maximum utilisation F/F_{allow}, defined against the allowable pressure, rises from 0.75 to a peak of 0.824 at $d = 2.5$ m, relaxes to 0.735 at $d = 4.5$ m as buoyancy takes over the aft part of the load, and then rises again to 0.769 at $d = 5.0$ m as the load shifts onto the forward bags. The ratio of reaction to rated capacity exceeds unity at one stage only, $d = 2.5$ m, where it reaches 1.022; the most heavily loaded bag is therefore worked marginally beyond its rated capacity but remains far below the ultimate capacity. The safety factor, defined as the sum of the allowable capacities of the bags in contact divided by the launching weight, decreases from 1.357 at $d = 0$ to 0.796 at $d = 5.0$ m and crosses the customary value of 1.2 between $d = 2.5$ m (1.207) and $d = 3.0$ m (1.163). The latter is therefore adopted as the governing stage in Sections 4.3 and 4.4: it is the first stage at which the system reserve falls below the customary threshold.

Figure 3a follows the bag that carries the highest utilisation. At rest the peak sits amidships, 64.0 m from the aft perpendicular, where the girder deflection is largest; once the hull starts to move the peak jumps to the last bag still on the ways and then tracks the slipway end, remaining 0.8–5.1 m inboard of it for stern drafts of 0.5–3.5 m. Above about 4 m the aft body floats, the remaining support shifts forward, and the peak moves to 143.9 m at 4.5 m draft and to the forwardmost bag at 239.85 m at 5.0 m. Panel (b) collects the two system-level quantities as continuous envelopes, with the six stages of Table 4 marked as open symbols: the margin above the minimum working height falls from 0.644 m at rest to a minimum of 0.385 m at 2.5 m draft and recovers to 0.706 m at 4.5 m, whereas the safety factor falls monotonically.

The contrast between the two indicators is itself informative. Local utilisation peaks by $d = 2.5$ m and then relaxes through the middle of the launch, whereas the system-level margin keeps falling, because the governing quantity late in the launch is the number of bags still able to carry load rather than the severity of the loading on any single bag. Assessing a launch by peak bag pressure alone would therefore miss the stage at which the reserve is actually smallest.

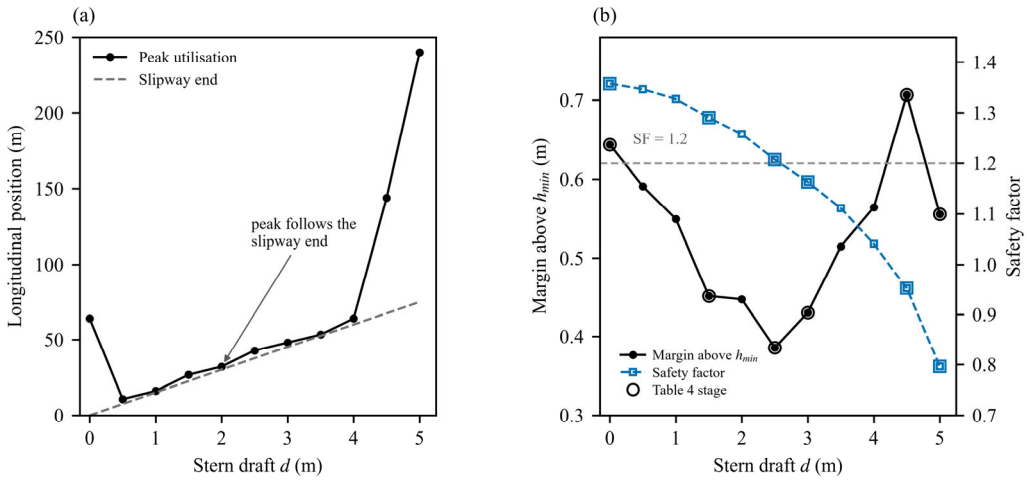

Figure 3. Stage evolution against stern draft: (**a**) longitudinal position of the peak bag utilisation and of the slipway end; (**b**) margin above the minimum working height and safety factor, with the six stages of Table 4 marked as open symbols.

Table 4. Support configuration and margins against stern draft.

d (m)	x_e (m)	Bags in Contact	Max Utilisation	F/F_{rated}	Min Height (m)	Margin (m)	SF	Buoyancy (MN)
0.0	0.0	45	0.747	0.691	1.244	+0.644	1.357	0.0
1.5	22.5	41	0.800	0.927	1.052	+0.452	1.290	7.1
2.5	37.5	38	0.824	1.022	0.985	+0.385	1.207	19.4
3.0	45.0	37	0.808	0.956	1.031	+0.431	1.163	28.3
4.5	67.5	33	0.735	0.622	1.306	+0.706	0.953	69.5
5.0	75.0	31	0.769	0.793	1.156	+0.556	0.796	95.0

4.2. Migration of the Unfavourable Support Position

The reaction profiles in Figure 4 show where the array is most severely worked. When the whole hull rests on the ways ($d = 0$) the profile is nearly uniform, running from 3.74 MN at the forward bags to 5.60 MN amidships, and the shallow maximum sits in the cargo-hold region ($x = 64.0$ m) as a result of the weight distribution. Once the stern begins to float, a marked peak appears immediately ahead of the slipway end: 7.51 MN at $d = 1.5$ m ($x = 26.6$ m), 8.28 MN at $d = 2.5$ m ($x = 42.6$ m) and 7.75 MN at $d = 3.0$ m ($x = 48.0$ m), while the reactions farther forward fall away. In each of these stages the peak sits between 0.8 and 5.1 m ahead of the slipway end, so its position follows the boundary rather than the hull. Beyond $d = 3.0$ m the peak begins to detach from the boundary as buoyancy spreads the load: at $d = 4.5$ m the maximum has moved to $x = 143.9$ m, and by $d = 5.0$ m it sits at $x = 239.8$ m, the aftermost bag still on the ways being relieved.

The mechanism is straightforward. The stub of hull aft of the slipway end is supported by buoyancy alone, so the bags still on the ways must carry the weight of that region through the shear and bending of the hull; the first bag behind the boundary is the point at which this transfer occurs, and it carries the concentration. The result is a support location that is not a property of the ship alone but of the launch stage, and it is this bag, not any amidships bag, that governs utilisation and height margin during the transition.

The peak also depends on how strongly the weight is concentrated amidships. Raising the peak-to-mean ratio of the weight distribution from 1.57 to 3.42 moves the maximum at $d = 0$ from $x = 5.3$ m (the aftermost bag) through $x = 64.0$ m to $x = 80.0$ m, so the weight distribution decides where the maximum sits while the hull is still fully supported. Once the stern floats, the boundary bag takes over in every case. The slipway end, rather than the weight distribution, is therefore the robust indicator of where to look during the transition.

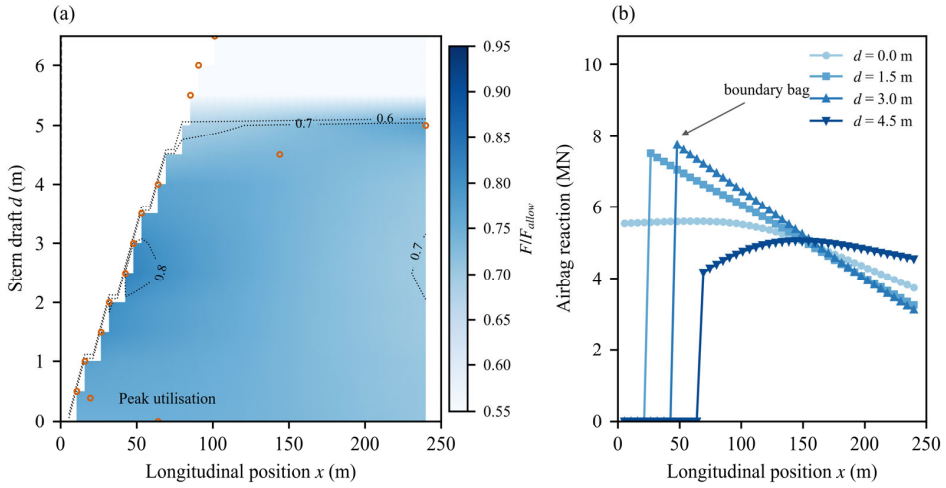

Figure 4. (**a**) Utilisation field over longitudinal position and stern draft, with the slipway end and the peak-utilisation ridge; (**b**) reaction profiles at four stages.

4.3. Load Redistribution After Gas Loss

Figure 5 compares four states at the governing stage $d = 3.0$ m: intact, gas loss with $\mu = 0.6$ on the most heavily loaded bag, and the two simplified variants of Section 2.5. The damaged bag is the one identified in Section 4.2, at $x = 48.0$ m with a reference height $h_{ref} = 1.031$ m.

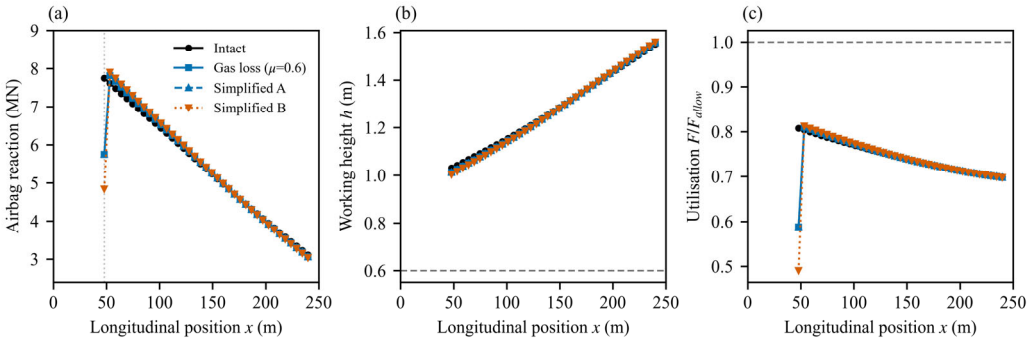

Figure 5. Four states at the governing stage: (**a**) airbag reaction; (**b**) working height; (**c**) utilisation. Only bags still on the ways are shown.

With 40% of the gas mass removed, the reaction of that bag falls from 7.747 MN to 5.745 MN, a loss of 25.8%, and its working height decreases by 19 mm. The neighbouring bags pick up the difference: the maximum utilisation among the remaining bags rises from 0.803 to 0.810, and the minimum working height over the supported bags falls by 19 mm, from 1.031 m to 1.012 m. The redistribution is therefore real but modest, because the thirty-six intact bags share the load that one bag has shed.

The redistribution is not confined to the immediate neighbourhood. Figure 6 plots the change in reaction of every bag. The bags adjacent to the damaged one gain up to 2.6%, and the largest increase is carried by the bag at $x = 53.3$ m, immediately forward of the damaged one. The increment decays along the length, changes sign at about $x = 150$ m, and the forward bags lose up to 1.7%. The reason is that the damaged bag settles by 19 mm and the hull pitches accordingly, which unloads the forward part of the hull. Gas loss therefore produces a global redistribution with a sign change along the length, not a local transfer between neighbouring bags, and a single-bag check cannot capture it.

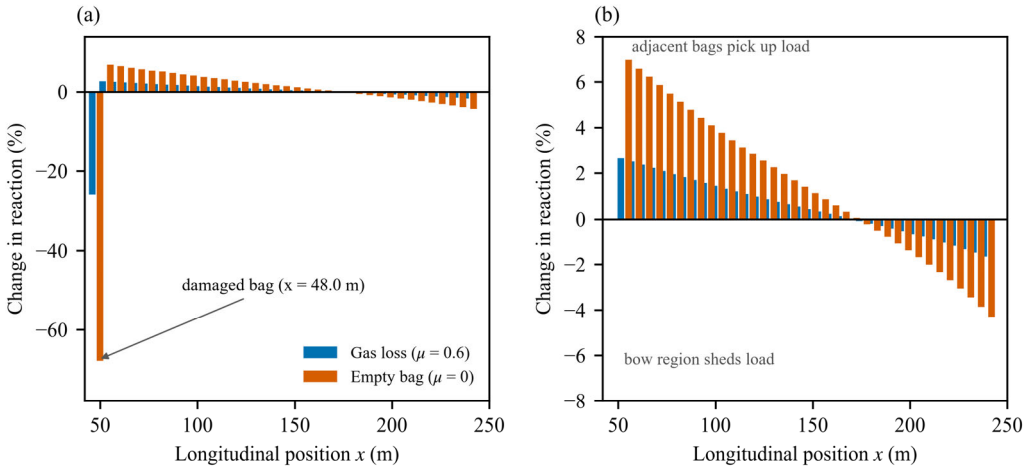

Figure 6. Change in reaction relative to the intact state at the governing stage: (**a**) whole array; (**b**) enlarged view of the remaining bags.

In the limiting case where all internal overpressure is removed from the same bag, Equation (5) provides an asymptotic bound in which the reaction does not fall to zero but to 2.49 MN, 32% of its original value, because the pressure-independent carcass term remains active under compression. Under this constitutive idealisation the bag settles by a further 49 mm, from 1.031 m to 0.982 m, and the stern of the hull drops by 71 mm relative to the intact state. This is the central quantitative result of the study: within this class of cord-reinforced support, the loss of internal gas pressure is not equivalent to the complete removal of the support, as the compressed carcass continues to act as a compliant elastic spring. It is a property of the linear carcass law over the deformation range in which that law was calibrated, 38% to 51% of the free diameter (Section 3.2); a bag whose reinforcement behaves nonlinearly at that compression would retain less, and no experiment on a depressurised bag exists to confirm the value (Section 5.4).

4.4. Comparison with the Simplified Capacity-Reduction Model

Simplified A, which matches the reduced capacity at h_{ref}, reproduces the gas-loss result almost exactly: 5.753 MN against 5.745 MN for the damaged bag, and essentially identical utilisation and height for the rest of the array. The reason was anticipated in Section 2.3. Equation (5) is the sum of a term proportional to μ and a term independent of it, and at a fixed height the ratio of the two is a constant; scaling the whole reaction by $\lambda_A = 0.7225$ therefore reproduces the curve closely, although not identically. The residual difference in the reaction, 0.13%, is the curvature mismatch over the 19 mm by which the bag settles.

Simplified B, which sets $\lambda_B = \mu = 0.6$, does not. It gives 4.837 MN for the damaged bag, 16% below the gas-loss model, and pushes the remaining bags to 0.813 utilisation instead of 0.810. Its working height is 1.004 m against 1.012 m. The error has a simple closed form: the capacity ratio predicted by treating gas loss as proportional is μ, whereas the true ratio is λ_A, and the difference $\lambda_A - \mu$ is precisely the fraction of the original reaction carried by the carcass. Figure 2b shows the two ratios over the whole range of μ: the gap widens as the loss increases, reaching one third of the reaction when the bag is empty.

The engineering consequence is a matter of conservatism. Simplified B understates the residual support of a damaged bag, so it overstates the load transferred to its neighbours and errs on the safe side, provided that the residual support is the quantity of interest. Where the question is instead whether a bag has failed in the sense of carrying nothing, as in a post-event assessment, Simplified B is misleading: a bag with no gas at all is still carrying a third of its design load and treating it as absent would distort the reconstructed load path.

4.5. Sensitivity to Multi-Bag Loss and to the Weight Distribution

Single-bag loss leaves the array with margin at the governing stage examined, so the sensitivity study addresses how much loss is needed before a limit is reached. Table 5 reports the governing stage $d = 3.0$ m with one, two, three, five and eight adjacent bags damaged, each at $\mu = 0.6$, 0.3 and 0.

With one bag emptied the utilisation of the remainder rises from 0.803 to 0.820 and the minimum height margin stays at +0.382 m, that is, 0.38 m above the 0.6 m floor. The margin is consumed as further bags are damaged: +0.331 m at two, +0.277 m at three and +0.164 m at five, before turning negative at eight (−0.014 m). Eight adjacent bags emptied therefore constitute the first case in which a limit is crossed, and the limit that is crossed is the minimum working height, not the bearing capacity; utilisation at that stage is still only 0.898.

Table 5. Sensitivity to multi-bag gas loss at the governing stage (d = 3.0 m).

Lost Bags n	μ	Max Utilisation (Others)	Min Height (m)	Margin (m)	Residual Force of Lost Bags (MN)
1	0.60	0.810	1.012	+0.412	5.7
1	0.30	0.815	0.997	+0.397	4.2
1	0.00	0.820	0.982	+0.382	2.5
2	0.60	0.811	0.994	+0.394	11.7
2	0.30	0.821	0.964	+0.364	8.6
2	0.00	0.833	0.931	+0.331	5.2
3	0.60	0.811	0.976	+0.376	17.7
3	0.30	0.826	0.930	+0.330	13.3
3	0.00	0.845	0.877	+0.277	8.1
5	0.60	0.810	0.944	+0.344	30.2
5	0.30	0.834	0.864	+0.264	23.4
5	0.00	0.869	0.764	+0.164	14.5
8	0.60	0.804	0.902	+0.302	49.3
8	0.30	0.836	0.774	+0.174	40.0
8	0.00	0.898	0.586	−0.014	25.6

This ordering matters for monitoring practice. Working height is a quantity that can be observed at the wayside, whereas the mobilised reaction of an individual bag cannot; the analysis indicates that the observable quantity is also the governing one.

The contiguous arrangement was chosen because it is the most severe one at a given number of lost bags, not because it is the most likely. The load released by a damaged bag is transferred to its immediate neighbours, because the hull distributes the deficit over a length of a few bag pitches: a group of adjacent losses concentrates that deficit on the two bags at the edges of the group, whereas the same number of losses separated by intact bags spreads it over twice as many survivors, each carrying a smaller increment. The transfer is also self-amplifying, since the neighbours of an emptied bag are the first to approach their height limit; adjacent loss is thus the arrangement produced by the failure mechanism itself rather than a scenario imposed beside it. The physical causes are correlated in the same way, a shared pressure manifold, a debris strike on the ways or a hull fitting acting on one region of the array rather than on scattered bags. Combinations of non-adjacent bags were therefore not enumerated. At a fixed number of lost bags the safety factor is governed mainly by how many bags remain in contact, whereas the arrangement-dependent indicators, local utilisation and minimum working height, are bounded by the contiguous case reported in Table 5; the limits of that bound, and of the quasi-static treatment, are stated in Section 5.4.

4.6. Robustness Across Hull Sizes

The prediction that the unfavourable support position follows the slipway end was obtained for one vessel, so the stage sequence was repeated for two further hulls with the same airbag system: 2.0 m × 18 m bags at 5.33 m pitch, the same constitutive model and the same rated capacity. Only the hull changes. Lengths are 190, 245 and 290 m, launching weights 127.5, 227.5 and 353.0 MN, and bending stiffnesses 1.0, 4.0 and 4.3 × 10^{13} N·m^2; the last was estimated from midship section proportions as $EI \propto BD^3$ and anchored on the 100,000 DWT case, so it reproduces relative stiffness rather than a specific vessel. Each sequence was run until buoyancy saturated the support, which for the smallest hull happens before d = 5.0 m. Table 6 summarises the results, and Figure 7 plots the two quantities that decide the question: the offset of the critical position and the severity of the loading on the most heavily worked bag.

Table 6. Robustness across hull sizes under an identical airbag array. W is the launching weight; the offset is measured from the slipway end to the position of maximum utilisation over d = 1.0–3.5 m; the last two columns give the safety factor at $d = 0$ and at the last converged stage.

Case	L (m)	W (MN)	Bags	Peak F/F_{allow}	Offset (m)	Max F/F_{rated}	pi	SF end
57k bulk	190	127.5	35	0.778	0.8–5.1	0.834	1.411	0.962
100k bulk	245	227.5	45	0.824	0.8–5.1	1.022	1.357	0.796
180k Capesize	290	353.0	53	0.914	0.8–5.1	1.336	1.284	0.956

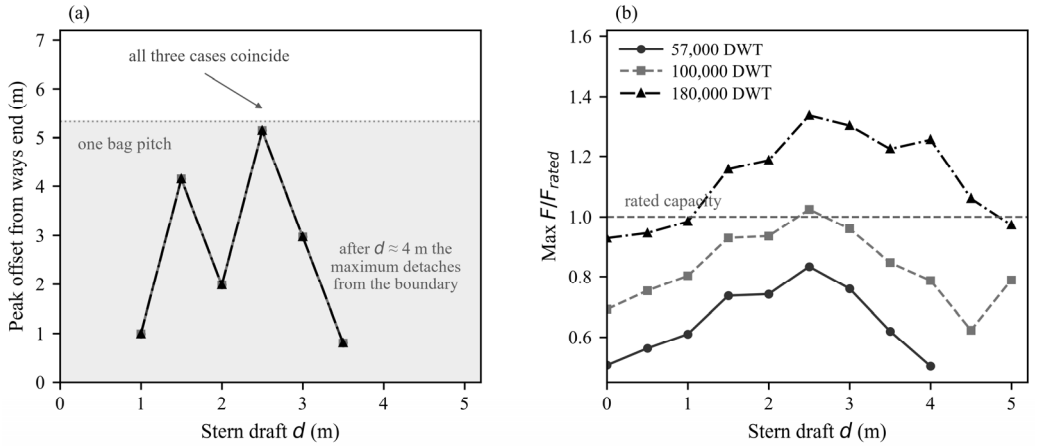

Figure 7. Robustness across hull sizes with an identical airbag array: (**a**) offset of the position of maximum utilisation from the slipway end, showing that the three cases coincide; (**b**) maximum reaction of a single bag relative to its rated capacity. Only the stages governed by the boundary are plotted in (**a**).

Between stern drafts of 1.0 and 3.5 m the position of maximum utilisation is identical for all three hulls: x = 16.0, 26.6, 32.0, 42.6, 48.0 and 53.3 m, that is 0.8–5.1 m ahead of the slipway end. The offset is set by the bag pitch rather than by the hull, because for a given draft the slipway end lies at $x_e = d/\tan\alpha$ and the peak falls on the first or second bag forward of it. The geometry of the critical position is therefore a property of the launch arrangement; only the magnitude of the loading depends on the ship.

The magnitude does depend on it. Peak utilisation rises from 0.778 for the 57,000 DWT hull to 0.824 and 0.914, and in the Capesize the most heavily loaded bag exceeds its rated capacity over the whole of d = 1.5–5.0 m, reaching 1.34. The same array therefore works with reserve on the smallest hull and is inadequate for the largest, which would need larger bags or a closer pitch. This is the quantitative form of the qualitative rule that bag capacity should be matched to hull weight.

Two smaller differences are worth recording. In the Capesize the maximum stays in the cargo-hold region until $d \approx$ 1.0 m, because buoyancy only becomes comparable with the local weight further into the launch, whereas the two smaller hulls have already transferred the peak to the boundary at d = 0.5 m. The draft at which buoyancy takes over the whole weight also grows with the hull: the 57,000 DWT case leaves the bag-supported phase between 4.0 and 4.5 m and the 100,000 DWT case at 5.5 m, while the Capesize still has 39 bags in contact at 5.0 m.

5. Discussion

5.1. Why Gas Loss Is Not a Loss of Capacity

Write the reaction of Equation (5) at a fixed height as $F = \mu F_g + F_c$, where F_g is the gas term and F_c the carcass term. The capacity ratio that a simplified model must reproduce is then

$$\frac{F}{F_0} = \mu + (1 - \mu)\,\frac{F_c}{F_g + F_c} \tag{13}$$

so that the excess over the gas ratio is the carcass share multiplied by the amount of gas lost. At the governing stage of the present case the carcass term carries 30.6% of the reaction of an intact bag at the reference height, and Equation (13) gives a capacity ratio of 0.723 (a 27.7% capacity loss) for $\mu = 0.6$, which matches Figure 2b and the numerical model. As the bag empties it settles further and F_c grows, so the residual ratio rises slightly, to 32% at $\mu = 0$. That figure belongs to the idealised carcass law and to the deformation range of Section 3.2, and not to the bag as a design component.

Equation (13) also defines when the simplification is exact: $\lambda_A = \mu$ if and only if $F_c = 0$. A support that relies on gas pressure alone, such as a thin air cushion without a load-bearing carcass, can legitimately be assessed by a proportional capacity reduction. A bag with eight cord layers cannot. The distinction is not a matter of modelling detail: at complete gas loss it changes the predicted residual support from a third of the design value to zero.

5.2. When the Simplified Method May Be Used

Simplified A reproduces the gas-loss result to 0.13% in reaction at the governing stage, so a proportional reduction is acceptable provided the factor is matched at a representative height. The practical difficulty is that this height is itself an output of the intact analysis, which makes the procedure iterative but not inaccurate.

Simplified B, taking the gas ratio as the capacity ratio, errs in a single direction: it understates the residual support of the damaged bag, by 16% at $\mu = 0.6$ and by a third of the intact reaction when the bag is empty. This is conservative for the question "will the remaining bags be overloaded", because the load transferred to them is overstated. It is not conservative for the question "how much support is left", and it is simply wrong if the damaged bag is to be represented in a reconstructed load path. Screening calculations that use Simplified B should therefore be reported as upper bounds on the transferred load rather than as estimates of the residual capacity.

5.3. Implications for Launching Practice

Three observations follow that are relevant to how a launch is monitored and arranged.

First, the governing quantity is the working height, not the mobilised reaction. In the multi-bag study, the bearing capacity was never approached: utilisation remained at 0.90 when eight bags were emptied, whereas the minimum working height crossed its limit at the same point. Working height can be observed at the wayside during a launch; the mobilised reaction of an individual bag cannot. The observable quantity is also the governing one.

Second, the critical bag is predictable. It is the first bag ahead of the slipway end, and its position follows the launch stage rather than the ship. Additional bags, or a reduced pitch, in that neighbourhood therefore act where they are needed, whereas uniform densification along the whole length spends material where utilisation is lower.

Third, a single-bag check is not sufficient in either direction. It is too optimistic in that it does not reveal the accumulated effect of several bags losing gas together, and it is too coarse in that the redistribution changes sign along the length: bags forward of about 60% of the length are unloaded rather than loaded. A check that looks only at the neighbours of the damaged bag would report the wrong trend for the forward part of the hull.

These observations translate into a procedure that can be run with the instrumentation a yard already has. Before the launch, the intact stage sequence identifies where and when the reserve is lowest and at which stern draught the customary factor is crossed, so that the monitoring effort can be concentrated on that length of the ways and on that stage of the move rather than spread uniformly. During the launch, the working height is measured at the wayside against its design floor; it is the limit reached first under multi-bag loss and it can be read without resolving the reaction of an individual bag. After a loss of gas is detected, the height to which the bag settles, entered in Equation (13), gives the support that the bag still contributes, and the proportional estimate is then used only as an upper bound on the load transferred to its neighbours. Each step relies on a quantity already recorded in a launch record. The results do not replace the intact-array check that governs the design [27]; they add the contingency layer that this check does not contain, and they indicate which measurement makes that layer usable.

5.4. Limitations

The carcass term in Equation (5) is linear in compression, which is calibrated for the moderate working range of the present launch stages (38% to 51% compression) but underestimates the nonlinear membrane lock-up of a nearly flattened bag by up to 42% at 62–83% compression, and does not model local shell buckling of an unloaded depressurised bag. Because the high-compression discrepancy grows only beyond about 60% deformation and errs on the conservative side for the damaged bag, it does not affect the support margins reported here, though a nonlinear high-compression law would be required if a bag were driven toward complete flattening. No published test has loaded a partially deflated bag against a hull bottom, so the gas-loss results are an extrapolation of this calibrated intact-bag law rather than an experimentally validated prediction. A dedicated test on a bag held at reduced internal pressure would be required to confirm the residual reaction; until such data exist, the residual fraction quoted in Section 4.3 should be read as a property of the present constitutive idealisation rather than as a design value.

The analysis is quasi-static and resolves vertical equilibrium at discrete launch stages. Slipway friction, longitudinal motion, bag rolling kinematics, the dynamic run-out after the hull leaves the ways and the transient following a bag burst are outside its scope. Referencing the slipway termination x_e to the waterline datum represents an effective support boundary at the water edge; where a submerged slipway apron extends below the waterline, the same boundary-transfer mechanism applies at the submerged way end. Buoyancy is integrated with an equivalent waterline breadth rather than the actual body plan, which affects the absolute distribution of load between water and bags but not the transfer mechanism discussed above. The damaged bag group is assumed contiguous, and non-adjacent losses are not examined.

The stage sequence stops at a stern draft of 5.0 m, where buoyancy already carries 42% of the launching weight. At larger drafts the floatation balance is reached, the bags unload completely and the waterline is no longer set by the bag reactions, so the stage formulation ceases to apply and no converged bag-supported solution exists. Within the reported range the waterline iteration was driven to a residual below 10^{-4} m; fixing the iteration count instead shifts the draft by up to 0.14 m and the peak utilisation by 0.04, which is why all values reported here are taken from the converged solutions.

Finally, the baseline vessel represents a standard bulk-carrier configuration with a continuous longitudinal weight profile whose peak-to-mean ratio is varied parametrically. The conclusions that depend on the weight profile, namely the position of the load maximum before the stern is afloat, were tested across a wide range of peak-to-mean ratios, while

vessels with highly localised mass concentrations, such as heavy deck modules, should be evaluated with their specific weight and stiffness distributions.

6. Conclusions

A quasi-static model of a hull supported by an array of airbags on an inclined slipway has been used to examine how gas loss from a single bag redistributes the vertical support and changes the remaining margin during a longitudinal launch. The following conclusions are drawn.

1. With an isothermal gas term and a carcass term calibrated on published model-scale tests, the model reproduces the manufacturer's rated capacity at 50% deformation to within 0.04%, using a stiffness that was fixed independently. The support model therefore rests on two consistent sources rather than on a single fitted parameter.
2. The most unfavourable support position is not a property of the ship. While the stern is flooding it migrates with the launch stage and stays 0.8–5.1 m ahead of the slipway end, where the hull load from the floating stern is transferred into the ways, so its position can be predicted from the slipway end rather than from the weight distribution. Repeating the stage sequence for 57,000, 100,000 and 180,000 DWT hulls with an identical bag array returns the same offsets, which identifies the position as a property of the launch arrangement. Only after buoyancy carries a third of the launching weight does the maximum detach from the boundary and move forward.
3. Gas loss is not equivalent to a proportional loss of bearing capacity. The capacity ratio follows $\mu + (1 - \mu)\, F_c/(F_g + F_c)$, where $F_c/(F_g + F_c)$ is the carcass share of the reaction; a fully deflated bag in the present case retains 32% of its original reaction, and a proportional reduction reproduces the gas-loss result only when the carcass term vanishes. This value is a result specific to the linear carcass idealisation and the deformation range of Section 3.2 rather than a general design rule.
4. Local utilisation and system reserve diverge along the launch. Utilisation peaks at 0.82 at a stern draft of 2.5 m and then relaxes as buoyancy takes over, whereas the capacity reserve falls throughout and crosses the customary factor of 1.2 at a stern draft of 3.0 m. Under multi-bag loss the first limit to be crossed is the minimum working height, at eight adjacent bags emptied, while bearing capacity remains below its limit.

Future work should extend the stage sequence to the dynamic run-out after the hull leaves the ways, and should include the transient following a bag burst, both of which are outside the quasi-static scope adopted here.

Author Contributions: Conceptualization, J.C. and S.B.M.; methodology, J.C.; software, J.C.; validation, J.C., S.B.M. and R.Y.; formal analysis, J.C. and R.Y.; investigation, J.C. and R.Y.; writing—original draft preparation, J.C.; writing—review and editing, S.B.M. and R.Y.; visualization, J.C. and R.Y.; supervision, S.B.M.; project administration, S.B.M. All authors have read and agreed to the published version of the manuscript.

Funding: This research received no external funding.

Data Availability Statement: The original contributions presented in this study are included in the article. Further inquiries can be directed to the corresponding author.

Conflicts of Interest: Author Rongtao Yang was employed by the company Anhui Port & Shipping Sealand Equipment Co., Ltd. The remaining authors declare that the research was conducted in the absence of any commercial or financial relationships that could be construed as a potential conflict of interest.

Nomenclature

Latin symbols	
$A(h)$	contact area between a compressed bag and the hull bottom (m^2)
$A_{cs}(h)$	cross-sectional area of the compressed bag section (m^2)
a	heave of the hull, i.e., its rigid-body vertical displacement (m)
B	moulded breadth of the hull (m)
$B(x)$	equivalent waterline breadth at station x (m)
b	pitch of the hull, i.e., its rigid-body rotation (rad)
$b(h)$	contact width of a compressed bag; distinct from the pitch b, the argument h identifying it (m)
C_b	block coefficient of the hull (–)
D	moulded depth of the hull (m)
D_b	free (uncompressed) diameter of a bag (m)
d	stern draft of the hull (m)
$EI(x)$	hull-girder flexural rigidity ($N{\cdot}m^2$)
f	consistent nodal load vector from self weight, bag reactions and buoyancy (MN)
$F(h)$	vertical reaction of a bag (MN)
$F_{allow,i}$	allowable reaction of bag i at its working height (MN)
F_i	mobilised reaction of bag i (MN)
F_{ult}	ultimate bearing capacity of a bag (MN)
F_0	reaction of an intact bag at the reference height (MN)
F_c	reaction component carried by the bag carcass at a given height (MN)
F_g	reaction component carried by the compressed gas at a given height (MN)
g	gravitational acceleration (m/s^2)
h	working height of a compressed bag (m)
h_i	working height of bag i (m)
h_{min}	minimum working height of a bag (m)
h_{ref}	reference working height (m)
J	tangent matrix of the residual vector, that is, its derivative with respect to the unknowns (–)
K	elastic stiffness matrix of the beam model (–)
k_s	carcass stiffness of the bag wall (Pa)
L	length between perpendiculars of the hull (m)
L_b	effective length of a bag (m)
M	bending moment resultant of the hull (MN·m)
m	current mass of gas in a bag, with m0 the initial value (kg)
N	number of airbags in the array (–)
p_0	initial internal pressure of a bag (MPa)
$p(h)$	internal pressure of a compressed bag (MPa)
p_{allow}	allowable internal pressure of a bag (MPa)
$q_b(x)$	buoyancy load per unit length of the immersed hull (kN/m)
q_{rated}	rated capacity per unit length of a bag (kN/m)
R	residual vector of the beam equilibrium equations (–)
$SF(d)$	safety factor of the support array at stern draft d, the sum of the allowable reactions divided by the launching weight (–)
SF_0	design safety factor on the rated capacity of a single bag (–)
s	longitudinal pitch of the airbag array (m)
u	vector of unknowns, collecting the nodal deflections and rotations together with the two rigid-body parameters (–)
$V(h)$	enclosed gas volume of a compressed bag (m^3)
V_0	initial enclosed gas volume of a bag (m^3)
W	launching weight of the hull (MN)
W_L	lightship weight of the hull (t)
$w(x)$	elastic vertical deflection of the hull (m)

x	longitudinal coordinate measured from the aft perpendicular (m)
x_e	position of the slipway end in hull coordinates (m)
x_g	longitudinal centre of gravity measured from the aft perpendicular (m)
x_{mid}	longitudinal coordinate of midship (m)
$Y(x)$	total vertical displacement of the keel line (m)
z_k	keel elevation (m)
z_w	waterline elevation (m)
Greek symbols	
α	slope angle of the slipway (rad)
δ_{max}	maximum allowable deformation of a bag (m)
θ	nodal rotation of the beam element (rad)
λ_A, λB	capacity-reduction factors of Simplified A and Simplified B (–)
μ	residual gas mass ratio of a damaged bag, m/m0 (–)
μ_i	local utilisation of bag i, that is, the ratio of its mobilised to its allowable reaction; distinct from the mass ratio μ by its bag index (–)
ρ	density of water (kg/m^3)
Acronyms	
AP	aft perpendicular
DWT	deadweight tonnes
MN	meganewton
SF	safety factor
URANS	unsteady Reynolds-averaged Navier–Stokes

References

1. Yu, L.; Li, Y.; Xia, L.; Ding, J.; Yang, Q. Research on Mechanics of Ship-Launching Airbags I—Material Constitutive Relations by Numerical and Experimental Approaches. *Appl. Ocean Res.* **2015**, *52*, 222–233. [CrossRef]
2. Thomas, J.-C.; Wielgosz, C. Deflections of Highly Inflated Fabric Tubes. *Thin-Walled Struct.* **2004**, *42*, 1049–1066. [CrossRef]
3. Brayley, K.E.; Davids, W.G.; Clapp, J.D. Bending Response of Externally Reinforced, Inflated, Braided Fabric Arches and Beams. *Constr. Build. Mater.* **2012**, *30*, 50–58. [CrossRef]
4. Clapp, J.D.; Young, A.C.; Davids, W.G.; Goupee, A.J. Bending Response of Reinforced, Inflated, Tubular Braided Fabric Structural Members. *Thin-Walled Struct.* **2016**, *107*, 415–426. [CrossRef]
5. Wu, W.; Yin, Y.; Li, Y.; Fan, X. Theoretical Analysis of Inflated Tube Wrinkling Behavior under Pure Bending. *Int. J. Mech. Sci.* **2024**, *273*, 109166. [CrossRef]
6. Davids, W.G. Behavior of Inflatable Drop-Stitch Fabric Panels Subjected to Bending and Compression. *Materials* **2023**, *16*, 6919. [CrossRef] [PubMed]
7. Davids, W.G.; McGlone, A.G. Impact of Shear Deformations on the Response of Inflated Drop-Stitch Fabric Panels Subjected to Transverse Loads. *Fibers* **2026**, *14*, 23. [CrossRef]
8. Ye, Y.; Gan, J.; Liu, H.; Guan, Q.; Zheng, Z.; Ran, X.; Gao, Z. Experimental and Numerical Studies on Bending and Failure Behaviour of Inflated Composite Fabric Membranes for Marine Applications. *J. Mar. Sci. Eng.* **2023**, *11*, 800. [CrossRef]
9. Liu, J.; Yu, L. Numerical Investigation on Nonlinear Contact Coupling during Ship Launching Process by an Array of Airbags. *Ocean Eng.* **2022**, *255*, 111481. [CrossRef]
10. Ren, H.; Li, C.; Feng, G.; Liu, X.; Zhang, J. Safety Assessment of Ship Launching Based on Airbags with the Nonlinear Rigidity of Airbags Being Considered. In *Proceedings of the ASME 28th International Conference on Ocean, Offshore and Arctic Engineering (OMAE2009)*; ASME: Honolulu, HI, USA, 2009; pp. 147–152. [CrossRef]
11. Bin Muhammad Saleh, A.; Gonawan, C.H.; Ikhwani, R.J.; Hidayat, T.; Habibi, H.; Suwedy, W. Numerical Investigation of the Laying of Airbag Arrangements on Launching Barges. *Int. J. Mar. Eng. Innov. Res.* **2023**, *8*, 202–212. [CrossRef]
12. Abdullah, K.; Sarena, S.T. Design of a Passenger Ship Launch Using an Air Bag System. *J. Teknol.* **2024**, *16*, 17–26. [CrossRef]
13. Dzulfiqar, M.A.; Pujo, N.F.; Pamungkas, N.; Husen; Mufariz, M.F.; Fadhilah, N. Studi Perhitungan dan Implementasi Airbag pada Peluncuran Kapal Tongkang 330 Feet Berdasarkan Standar CB/T 3837-1998 [Calculation and Implementation of Airbags in the Launching of a 330 ft Barge Based on Standard CB/T 3837-1998]. *J-ENSITEC* **2024**, *11*, 10131–10136. [CrossRef]
14. Noegraha, A.D.; Djamaluddin, R.; Irmawaty, R.; Sitepu, G. Study of the Effect Launching System Using Airbags on the Hull Structures of Pinisi Ship. *J. Adv. Res. Appl. Sci. Eng. Technol.* **2024**, *49*, 278–295. [CrossRef]

15. Sugeng, S.; Ridwan, M.; Suharto, S.; Khristyson, S.F. Technical and Economic Analysis of Ship Launching with Slipway and Airbag KM. Sabuk Nusantara 72 in PT. Janata Marina Indah Shipyard Semarang. *Teknik* **2020**, *41*, 225–231. [CrossRef]
16. Mahendro, I.; Affariz, N. Use of the Marine Airbag Ship System in the Slipway Area of the Shipyard. *J. Sains Teknol. Transp. Marit.* **2024**, *6*, 45–50. [CrossRef]
17. Ramzi, M. Automatic Procedure of Side Ship Launching Calculation. *Ann. Dunărea Jos Univ. Galați Fasc. XI Shipbuild.* **2018**, *41*, 133–138. [CrossRef]
18. Volenyuk, L.; Rashkovskyi, A. Ship Stability Analysis during Launching from Longitudinal Sloping Slipway by Pneumatic Airbags. *Int. Shipbuild. Prog.* **2017**, *64*, 41–50. [CrossRef]
19. Liu, K.; Wang, Y.; Wu, Z.; Pi, J.; Gho, W.M.; Zhou, B. Numerical Simulation on Dynamic Characteristics of Longitudinal Launching of Large Container Ships. *J. Mar. Sci. Eng.* **2022**, *10*, 1583. [CrossRef]
20. Chen, S.; Li, M.; Liu, Y.; Bai, X. Data-Driven Approach to Safety Control in Jacket-Launching Installation Operations. *J. Mar. Sci. Eng.* **2025**, *13*, 554. [CrossRef]
21. Žgomba, D.; Turk, A.; Hadjina, M.; Hadjina, D.; Margić, I. Longitudinal Ship Launching. *J. Marit. Transp. Sci.* **2020**, *3*, 239–249.
22. Cui, H.; Chen, Z.; Hu, R.; Ding, Q. Ultimate Strength Assessment of Hull Girders Considering Elastic Shakedown Based on Smith's Method. *Ocean Eng.* **2024**, *293*, 116695. [CrossRef]
23. Akyıldız, H.; Menteş, A. Risk Assessment of Launching Airbags Using Functional Resonance Accident Model. *Trans. Marit. Sci.* **2023**, *12*, 005. [CrossRef]
24. Walker, F.K. An Overview of Ship Launching. In *Drydocks, Launching & Shiplift*; RINA: London, UK, 2003; pp. 83–90. [CrossRef]
25. Rashkovskiy, S.A.; Rashkovskyi, A.A. Rolling Resistance of Marine Airbags at the Longitudinal Inclined Slipway during Ship Launching. *Int. Shipbuild. Prog.* **2014**, *61*, 41–59. [CrossRef]
26. Antonenko, S. Selection of Optimal Keel Block for Docking Ships with Large Bow and Stern Overhangs. *Trans. Krylov State Res. Cent.* **2020**, *S-I*, 57–62. [CrossRef]
27. *ISO 14409:2011*; Ships and Marine Technology—Ship Launching Air Bags. International Organization for Standardization: Geneva, Switzerland, 2011.
28. Liu, J.; Yu, L.; Li, X.; Liu, J. Numerical Investigation on Blasting Failure and Impact Effects of Marine Launching Airbags. In Proceedings of the International Conference on Computational & Experimental Engineering and Sciences (ICCES), Singapore, 3–6 August 2024; Volume 29. [CrossRef]
29. Li, H.; Fang, X.; Yu, L. Research on Safety of Ship Launching with Airbags under Extreme Condition of Airbag Explosion. *Ship Eng.* **2017**, *39*, 59–63, 79. (In Chinese)
30. Sato, M.; Kanie, S.; Mikami, T. Mathematical Analogy of a Beam on Elastic Supports as a Beam on Elastic Foundation. *Appl. Math. Model.* **2008**, *32*, 688–699. [CrossRef]
31. Zemskov, A.V.; Tarlakovskii, D.V. Unsteady Elastic Diffusion Bending Model for a Timoshenko Beam on a Winkler Foundation. *Arch. Appl. Mech.* **2022**, *92*, 1355–1366. [CrossRef]
32. Ivanov, L.D. Hull Girder Elastic Section Modulus as a Representative of Hull Girder Geometric Properties in Probabilistic Analyses. *Ship Technol. Res.* **2012**, *59*, 22–35. [CrossRef]
33. Li, S.; Kim, D.K.; Ringsberg, J.; Liu, B.; Benson, S. Uncertainty of Ship Hull Girder Ultimate Strength in Longitudinal Bending. *Int. J. Marit. Eng.* **2022**, *164*, 185–206. [CrossRef]

Disclaimer/Publisher's Note: The statements, opinions and data contained in all publications are solely those of the individual author(s) and contributor(s) and not of MDPI and/or the editor(s). MDPI and/or the editor(s) disclaim responsibility for any injury to people or property resulting from any ideas, methods, instructions or products referred to in the content.